Astron. Astrophys. 235, 103–113 (1990)

ASTRONOMY AND ASTROPHYSICS

Blue Magellanic clusters: near-infrared spectral evolution*

E. Bica[1], D. Alloin[2], and J.F.C. Santos Jr.[1]

[1] Universidade Federal do Rio Grande do Sul, Departamento de Astronomia, Av. Bento Gonçalves, 9500, 91500 Porto Alegre, RS, Brazil

[2] Observatoire de Paris, Section de Meudon, URA 173 CNRS, 5, Place Jules Janssen, F-92195 Meudon, France

Received October 12, accepted December 19, 1989

Abstract. We present new integrated spectra in the range 5600–10 000 Å for 28 LMC and 3 SMC young star clusters. We measure the equivalent widths (W) of prominent features and the continuum distribution. The analysis, supplemented by 8 additional LMC clusters from our previous studies, indicates that the red supergiant phase is indeed very time-peaked, occuring from 7 to 12 Myr. In addition to the previous case of NGC 2004, we find that NGC 1805, NGC 1994, NGC 2002, NGC 2098 and NGC 2100 as well as NGC 2011 to a lesser extent, are undergoing this phase. The red supergiant phase is clearly denoted by strong TiO bands and Ca II triplet as well as a flat continuum or in extreme cases a continuum with positive slope for $\lambda > 6000$ Å. In the SMC clusters, the molecular bands are weak, owing to metal deficiency, but we can show nevertheless that NGC 299 clearly belongs to the red supergiant phase as demonstrated by its spectral slope and enhanced Ca II. We also find new evidence of another red phase at $t \approx 100$ Myr, possibly produced by AGB stars, in which the clusters NGC 2031 and NGC 2134 exhibit strong molecular bands like NGC 1866, a previously known case. Clusters between 10 and 50 Myr have strong Hα emission arising from Be stars, a phenomenon which occurs also in Galactic open clusters. From the LMC data set, it has been possible to identify 8 stages in the cluster spectral evolution from 5 to 500 Myr. We derive the corresponding average spectra which shall be useful for population synthesis of galaxies in which recent bursts of star formation have occurred.

Key words: star clusters – Magellanic Clouds – red supergiants – stellar evolution – spectral evolution

1. Introduction

Blue Magellanic clusters of a globular appearance are populous objects with integrated colours $(B-V)<0.4$, which basically correspond to ages younger than a few 10^8 yr. Since the early study by Hodge (1961), analyses of their integrated light and HR diagrams have provided valuable information in the stellar content, dynamics and chemical evolution of the Clouds (Searle, Wilkinson and Bagnuolo, 1980, hereafter SWB80; van den Bergh, 1981; Cohen, 1982; Hodge, 1983; Freeman et al., 1983). They impose important constraints on the stellar evolution theory (Chiosi et al., 1988) and are very useful for population synthesis of galaxies with recent bursts of star formation (Bica, 1988).

The evolution of their integrated light is very simple at short wavelengths: it can be merely described by the gradual disappearance of upper main sequence stars with minor influence of their later evolutionary stages (Cohen et al., 1984). On the other hand, in the infrared the integrated light behaviour as a function of age is very complex. The JHK photometry shows the need for red supergiants to explain the colours of very young clusters (Persson et al., 1983). Bica and Alloin (1986, 1987; hereafter BA86 and BA87) using visible and near-infrared spectra have confirmed the red-supergiant effect in NGC 2004 at $t \approx 10$ Myr and have also found an important red stellar content for NGC 1866 at $t \approx 100$ Myr. Evidence for the latter red phase can also be seen in the composite HR diagrams of Galactic open clusters (Mermilliod, 1981a,b). Arimoto and Bica (1989) have compared the photometric properties of young LMC clusters with a model of star cluster evolution including red supergiant tracks from classical stellar evolution models. The model, computed with a fine age step, produces a short red-supergiant phase at $t \approx 10$ Myr. Another type of red stars shows up for clusters between $20 < t\ \mathrm{Myr}^{-1} < 200$. Such stars are certainly AGB stars from intermediate mass ($\approx 6 M_{\odot}$) progenitors (Chiosi et al., 1988).

In order to provide new constraints on the red stellar content of young clusters and the related implication on modeling of their integrated light, we have increased through the present study, the number of blue Magellanic clusters with available near-infrared spectra. The total sample now contains 39 among the brightest and largest young clusters in the Clouds. In Sect. 2 we describe the observations and present the measurements. In Sect. 3 we make a comparative analysis of various spectral features and of the continuum slope. We also compare the present spectral results with those from infrared photometry. In Sect. 4 we derive an homogeneous set of age estimates for these clusters using the available HR diagrams and integrated colours from the blue-violet range. On the basis of these ages we then analyze the near-infrared spectral evolution. We identify eight spectral stages and generate the corresponding average spectra which will be useful for population synthesis of galaxies having suffered recent bursts of star formation (Sect. 5). Concluding remarks are given in Sect. 6.

Send offprint requests to: D. Alloin

* Based on data collected at the European Southern Observatory

2. Observations

Spectral observations in the range 5600 to 10 000 Å were carried out on nights 1988 January 14 and 15, at the Cassegrain focus of the ESO 1.52m telescope at La Silla coupled to a Boller and Chivens spectrograph. The detector was ESO CCD No. 13, which is a high resolution backside illuminated RCA SID 503 chip. We have used it in a size-limited configuration of 512 × 320 pxl with size 30μm × 30μm. The dispersion was 300 Å mm^{-1}, which, together with a slit width of 5″ produced a resolution of $\approx$14 Å as measured by the FWHM of comparison helium-argon lines. A filter OG 550 was necessary to block the second order contamination. Typical exposures ranged from 10 to 20 min for the clusters and 5 to 10 min for the standard stars EG 21, LTT 3218, Hiltner 600 and HD 117 880 for flux calibration and atmospheric absorption correction. The slit was set in the E-W direction and its length covered $\approx$3′ on the sky.

In order to have a good sampling of their stellar content, the observational technique for the star clusters consisted in scans along the N-S direction, which covered 20″ to 60″ on the sky depending on the cluster size. The reductions were performed at La Silla with the IHAP package and consisted in:

(i) Bias and flat-field corrections; the use of dome flat-fields at positions similar to those of the objects allowed the elimination of interference fringes by simple division.

(ii) Object and sky extraction: pixel rows in the range 15″ to 100″ were summed up depending on the cluster size while the sky rows were averaged sufficiently far from the center on each side, to avoid any cluster contamination.

(iii) Sky subtraction and wavelength calibration.

(iv) Correction for atmospheric extinction and flux calibration.

(v) Correction for O_2 and H_2O atmospheric absorptions using hot stars as described in detail in BA87.

The sample of blue star clusters consists in the largest and/or brightest ones in the Magellanic Clouds. They are 28 in the LMC and 3 in the SMC and are listed in Table 1 together with the corresponding sky area covered by the N-S scans and the E-W sums of pixel rows. We also complement the present observations with 8 additional clusters from our previous visible and near-infrared studies (BA86 and BA87), which are denoted by an asterisk in column 1. We have also compiled in Table 1 information available from the literature, where the colours were homogeneously corrected for foreground reddening, $E(B-V)=0.03$ and 0.06, respectively for the SMC and the LMC (Mould and Aaronson, 1980). Although estimates of the internal reddening exist in the literature we chose not to correct for internal reddening, as one of our objectives is to derive templates for population synthesis in galaxies, where it is suitable to keep the intrinsic reddening in the elements of the base (Bica, 1988).

We have verified the homogeneity of the spectral properties throughout the cluster surface by extracting the pixel rows corresponding to the eastern and western halves. In most cases the spectra are very similar, but in some clusters, e.g. NGC 2011, one part is much redder indicating either an inhomogeneous internal reddening or that the red stars are more concentrated in it. A similar effect occurs for the emission in some clusters. This suggests that for certain types of luminous, rare stars we might be at the threshold of the statistical significance of the properties for individual clusters. This is why in Sect. 5 we group the spectra within the same age range, so that possible statistical fluctuations are minimized.

We have searched for extended emission nebulae associated to the clusters in our sample on the Hα plates and catalogue of Davies, Elliot and Meaburn (1979, hereafter DEM) and Henize (1956). Interestingly, only the two largest and supposedly most massive clusters in the LMC and the largest one in the SMC have extended emission. In the LMC, NGC 1850 is associated to DEM 84 = Henize 103; NGC 2100 is superimposed on an anonymous nebula, which might be, however, a filament of the 30 Dor complex. The spectrum of NGC 1854 contains [S II] λ6716, λ6731 Å which arises from filaments in the nearby H II region NGC 1858 = DEM 86. In the SMC, NGC 330 is embedded in DEM 87.

Most of the emission in the cluster spectra appears to arise from stellar sources. Several clusters include an emission star from Henize's catalogue: S 3 at the S-E edge of NGC 1735, S 43 at the E edge of NGC 2004, S 145 in NGC 2214. In the case of NGC 1994 the star S 111 at the cluster edge has Ca II in emission and extremely strong Hα. We have excluded the pixel rows corresponding to this star, as they would have produced a very atypical integrated spectrum.

The measurements of equivalent widths (W) and continuum points follow the window definitions and continuum tracings given in BA86, BA87 and Bica and Alloin (1988). The measurements of the main molecular and atomic absorptions, as well as the particular case of Hα which often appears in emission are presented in Table 2. A selection of continuum points relative to that at 5870 Å are given in Table 3. Tables 2 and 3 include data for the new clusters only, while corresponding values for the eight previous clusters are to be found in BA86 and BA87.

3. Comparison of infrared observables

The molecular and atomic absorptions as well as the continuum distribution depend on the relative contributions to the integrated spectrum of stars with various spectral types and luminosity classes. Molecular bands appear preferentially in cool stars (mostly M type). Excellent correlations exist among equivalent widths of the various TiO bands, e.g. for the bands 7100 Å and 6300 Å in Fig. 1a. Absorptions from different molecules such as CN and TiO are well correlated (Fig. 1b). The continuum slope and the molecular absorptions are correlated as well (Fig. 1c).

A relationship between the equivalent widths of metallic lines (e.g. Na I D 5890 Å and Ca II 8542 Å) is presented in Fig. 1d. These lines originate not only in M but also in intermediate temperature stars, e.g. the Ca II triplet shows up from F to M stars (Jones et al., 1984). They are also correlated to molecular bands (Fig. 1e). It should be noted that the continuum tracing criterion used here, aims at measuring all the absorption in a window (BA86; BA87). So, part of the absorption in the Ca II and Na I windows are from TiO, which can amount to $\approx$50% in the clusters with red supergiants. A detailed analysis of the Ca II triplet with low continuum tracing and corrected for Paschen contamination is given in Sect. 5.

Some atomic lines in the near-infrared, such as the hydrogen Paschen series, arise in stars of B and A spectral types. We show in Fig. 2a the correlation between P 12 and P 14. A similar behaviour should be expected from Hα in absorption, however Hα in emission from B star envelopes is quite strong in many clusters and may contaminate significantly the absorption. Consequently no clear correlation appears (Fig. 2b). The extreme cases of absorptions arising from hot stars (Paschen) on one side and very

Table 1. Parameters for the cluster sample

(1) Cluster NGC	(2) Region NS-EW	(3) CO	(4) $(J-K)_0$	(5) Turnoff age (Myr)	(6) $(U-B)_0$	(7) $(B-V)_0$	(8) SWB	(9) $(u-v)_0$	(10) Age (Myr)
299	30″ × 30″	0.195	0.84	—	−0.46	0.24	I	−0.28	12
330	40 × 85	0.150	0.76	7	−0.46	0.14	I	−0.11	13
376	30 × 35	0.120	0.66	—	−0.42	0.24	I	−0.04	20
1711	40 × 60	0.115	0.46	—	−0.41	0.06	II	−0.05	20
1735	25 × 40	—	—	—	−0.32	0.06		—	32
1755	40 × 65	0.090	0.47	—	−0.25	0.09	II–III	0.21	55
1767	20 × 40	0.250	0.42	—	−0.64	0.14		—	7
1774	20 × 35	0.145	0.68	—	−0.31	0.14	II	0.11	37
1782	20 × 60	—	—	—	−0.29	0.20		—	36
1805	30 × 25	0.235	0.94	—	−0.59	0.05		—	9
1818	30 × 55	0.185	0.83	17	−0.51	0.12	I	−0.14	14
1831*	60 × 60	0.000	0.62	190	0.09	0.28	V	0.40	186
1847*	60 × 60	—	—	16	−0.37	0.14		—	21
1850	45 × 75	0.105	0.60	40	−0.39	0.06		—	31
1854	40 × 85	0.035	0.51	30	−0.26	0.15	II	0.05	34
1856*	60 × 60	0.065	0.53	120	0.03	0.28	IV	0.42	151
1866*	60 60	0.090	0.66	80	−0.08	0.19	III	0.26	86
1868*	30 × 60	0.180	0.66	500	0.11	0.39		—	500
1903	30 × 55	—	—	—	−0.29	0.08	II	0.16	44
1951	30 × 50	0.140	0.58	—	−0.23	0.03		—	48
1994	20 × 15	0.145	0.91	7	−0.73	0.10		—	6
2002	40 × 45	0.240	0.84	—	−0.61	0.31		—	8
2003	20 × 45	—	—	—	−0.64	−0.04		—	7
2004*	60 × 60	0.240	0.92	8	−0.72	0.11	I	−0.37	6
2006	20 × 40	—	—	—	−0.72	−0.09		—	5
SL 538	20 × 35	—	—	—	−0.69	0.04		—	6
2011	20 × 50	0.235	0.89	6	−0.76	−0.06		—	5
2025	25 × 55	—	—	—	−0.11	0.18		—	83
2031	40 × 85	—	—	—	−0.09	0.21		—	91
2041	40 × 50	0.080	0.53	—	−0.21	0.16	III	0.20	58
2058	30 × 85	0.165	0.63	70	−0.16	0.18	III	0.15	62
2065	30 × 80	0.040	0.45	70	−0.14	0.20	III	0.17	66
2098	40 × 50	—	—	—	−0.62	0.10		—	8
2100	60 × 100	0.240	1.00	10	−0.60	0.10	I	−0.27	9
2134	20 × 70	0.105	0.51	130	−0.06	0.19	IV	0.37	124
2136	40 × 50	0.100	0.56	—	−0.17	0.22	III	0.23	58
2157*	30 × 60	0.055	0.64	—	−0.20	0.13		—	42
2164	40 × 50	0.055	0.37	—	−0.28	0.04	III	0.12	44
2214*	60 × 60	0.170	0.73	40	−0.31	0.05	II	0.10	38

Columns: (1) NGC or SL designation; an asterisk denotes those clusters studied in Bica and Alloin (1986; 1987). (2) Area observed: N-S scan and E-W pixel rows. (3) and (4) CO and $(J-K)_0$ indices from Persson et al. (1983); $(J-K)$ and all other colours in this paper are corrected only for foreground reddening (Section 2). (5) Age from the HR diagram (Hodge, 1982; 1983). (6) and (7) *UBV* colours from van den Bergh (1981). (8) and (9) SWB classification and Gunn system colour from Searle et al. (1980). (10) Calculated average age (Section 4); for the blue/red transition cluster, NGC 1868, we adopted that of column (5).

cool ones (TiO) on the other side, are uncorrelated, as expected (Fig. 3).

We conclude that the stellar contributions in blue clusters produce quite complex combinations in the near-infrared and it is thus necessary to use independent age indicators for a detailed understanding of the integrated light evolution.

The present near-infrared observables associated with cool stars are reasonably correlated with colour indices from the infrared photometry of Persson et al. (1983). We show in Fig. 4a, TiO vs. CO, and in Fig. 4b, the near-infrared spectral slope vs. the $(J-K)_0$ colour: they indicate that basically the same types of red stars are responsible for the flux at $\lambda \approx 0.7\mu$m and $\lambda \approx 2.0\mu$m.

1990A&A...235..103B

Table 2. Equivalent widths for the new sample

(1) Cluster NGC	(2) 48 5897/34 Na I	(3) 49–51 5985/142 TiO	(4) 54–57 6271/230 TiO	(5) 59 6507/66 Ca I+Fe I	(6) 60 6563/46 Hα	(7) 66–68 7257/414 TiO	(8) 71 7778/148 TiO	(9) 72 7946/188 CN	(10) 75–76 8355/242 TiO	(11) 77 8498/44 Ca II+TiO	(12) 78 8542/44 Ca II+TiO	(13) 79 8602/76 P 14+TiO	(14) 80 8670/60 Ca II+TiO	(15) 81 8743/86 P 12	(16) 83–84 8955/222 P 10+P 11
299	2.3	3.9	13.0	1.1	−3.0	17.5	−0.4	4.5	11.7	3.3	6.1	2.1	4.3	1.7	4.1
330	1.5	2.1	8.1	0.4	−1.0	6.5	0.7	2.3	13.6	2.8	4.8	2.8	3.4	4.8	10.4
376	1.3	1.9	7.3	0.3	−1.9	9.6	−0.5	2.3	11.3	2.9	5.6	2.7	3.5	2.7	4.7
1711	1.3	2.5	6.4	0.6	−0.9	5.9	4.1	8.7	16.6	3.8	5.9	4.6	5.5	5.5	6.3
1735	0.6	0.6	4.3	0.1	−13.1	11.6	7.3	7.8	14.1	3.6	5.8	5.5	3.9	6.7	19.4
1755	1.1	1.9	7.2	1.1	2.2	11.1	2.7	4.6	12.7	3.6	4.8	2.5	4.5	5.1	13.4
1767	1.9	2.8	11.2	0.9	0.7	16.7	2.5	5.6	10.9	2.9	5.0	1.9	3.3	4.2	8.5
1774	1.7	1.7	7.3	0.2	2.9	14.9	1.0	5.0	13.1	3.9	6.3	3.7	4.8	4.8	10.4
1782	2.2	3.6	11.9	1.0	1.8	16.1	0.8	5.7	11.6	2.8	6.4	1.3	3.6	1.3	4.0
1805	4.8	12.0	31.8	2.9	3.5	70.8	30.3	25.0	23.9	9.1	10.7	7.8	7.7	4.4	11.2
1818	1.5	1.6	10.7	1.0	−0.1	12.5	0.7	4.8	14.1	3.5	6.8	4.1	5.9	5.7	10.1
1850	1.3	2.5	7.3	0.5	−7.0	11.0	3.2	7.1	18.8	2.8	4.2	3.7	5.1	5.3	21.7
1854	1.4	3.7	10.2	1.4	−13.7	16.6	1.8	6.0	22.3	5.4	6.2	5.8	8.1	7.9	22.1
1903	2.2	4.1	13.3	1.3	1.7	22.9	5.6	6.0	12.8	3.8	5.7	3.1	4.6	5.1	13.3
1951	2.3	4.2	11.9	0.8	−1.7	15.5	2.0	5.9	14.0	4.5	6.6	4.3	6.1	5.7	10.0
1994	3.0	5.7	19.9	0.9	−13.1	37.4	8.9	10.4	12.6	3.5	4.9	2.0	2.9	1.5	10.4
2002	3.7	7.3	23.8	2.0	−0.9	43.5	14.4	15.1	20.5	6.9	9.3	6.9	8.7	6.8	13.2
2003	1.0	0.7	5.9	0.4	2.5	11.0	4.6	7.3	14.1	4.4	5.1	7.0	6.2	8.0	19.3
2006	1.2	3.3	8.4	0.8	−1.5	12.7	3.4	8.1	14.3	4.5	6.5	4.2	4.0	7.9	17.0
SL 538	1.7	2.4	9.3	0.7	1.0	10.1	3.2	5.9	10.1	3.2	4.7	2.4	4.6	4.1	11.5
2011	2.0	3.4	13.3	1.0	1.1	23.2	8.5	8.4	14.8	4.1	5.9	3.6	4.9	5.3	14.0
2025	0.9	0.2	1.5	−0.3	1.6	6.0	2.0	3.6	13.2	3.7	6.1	4.0	5.0	6.4	12.5
2031	2.0	5.4	22.5	0.5	3.7	17.4	8.1	13.6	22.0	5.1	7.3	4.7	5.1	6.1	11.4
2041	1.2	0.6	5.2	−0.1	2.4	3.2	1.2	3.4	11.3	3.4	5.5	1.4	4.2	3.5	9.6
2058	1.6	2.2	6.5	0.3	3.3	11.5	3.3	3.5	12.6	4.2	5.5	3.9	4.2	5.0	13.4
2065	1.6	1.9	5.7	0.6	3.5	11.0	3.3	8.5	20.0	4.3	6.7	6.5	6.8	6.9	25.0
2098	2.5	4.8	16.1	1.8	−2.4	24.5	3.7	5.7	13.2	4.9	6.8	4.4	5.4	5.3	8.4
2100	3.1	5.0	16.3	1.1	−5.7	24.6	5.3	8.8	12.2	4.0	5.3	2.9	3.8	3.8	8.6
2134	1.4	2.3	9.9	1.2	4.5	22.9	6.8	5.3	11.1	4.3	5.7	4.6	4.6	5.2	7.7
2136	2.6	2.5	7.6	0.6	1.9	10.4	1.5	7.3	10.4	2.7	5.2	2.3	3.8	2.8	12.3
2164	0.9	2.3	5.2	0.2	1.9	8.8	3.2	6.1	16.0	4.1	5.9	5.5	5.4	6.2	26.5

Columns: (1) Cluster designation. (2) to (16) Equivalent widths in angstroms following window definitions from Bica and Alloin (1986; 1987). In column (6) negative values indicate emission. In the headings we provide the window number (second line), the median wavelength and the window width (third line) as well as the main contributing absorbers (fourth line).

Table 3. Continuum distribution for the new sample

(1) Cluster NGC	(2) $\frac{C(6630)}{C(5870)}$	(3) $\frac{C(6990)}{C(5870)}$	(4) $\frac{C(7520)}{C(5870)}$	(5) $\frac{C(8040)}{C(5870)}$	(6) $\frac{C(8408)}{C(5870)}$	(7) $\frac{C(8700)}{C(5870)}$	(8) $\frac{C(9100)}{C(5870)}$
299	0.99	0.97	0.95	0.93	0.92	0.90	0.89
330	0.81	0.74	0.66	0.59	0.57	0.56	0.54
376	0.86	0.80	0.74	0.69	0.67	0.65	0.63
1711	0.75	0.66	0.57	0.52	0.49	0.46	0.46
1735	0.75	0.66	0.60	0.54	0.51	0.51	0.51
1755	0.78	0.69	0.60	0.54	0.51	0.49	0.49
1767	0.79	0.72	0.65	0.59	0.56	0.55	0.54
1774	0.81	0.75	0.68	0.61	0.60	0.60	0.60
1782	0.83	0.76	0.71	0.65	0.62	0.61	0.59
1805	1.04	1.10	1.36	1.40	1.45	1.49	1.60
1818	0.82	0.75	0.69	0.64	0.63	0.63	0.63
1850	0.77	0.69	0.60	0.54	0.50	0.48	0.48
1854	0.78	0.71	0.63	0.56	0.54	0.52	0.52
1903	0.81	0.75	0.72	0.65	0.62	0.61	0.61
1951	0.80	0.73	0.69	0.65	0.63	0.63	0.64
1994	0.85	0.82	0.80	0.73	0.69	0.66	0.66
2002	0.99	1.01	1.09	1.09	1.13	1.17	1.22
2003	0.75	0.67	0.58	0.52	0.50	0.50	0.50
2006	0.75	0.66	0.58	0.52	0.49	0.48	0.49
SL 538	0.76	0.68	0.62	0.57	0.54	0.53	0.55
2011	0.81	0.74	0.70	0.75	0.63	0.63	0.65
2025	0.79	0.71	0.74	0.58	0.56	0.56	0.56
2031	0.97	0.88	0.84	0.78	0.77	0.77	0.78
2041	0.81	0.74	0.68	0.63	0.61	0.60	0.61
2058	0.78	0.71	0.64	0.57	0.55	0.53	0.52
2065	0.80	0.73	0.65	0.59	0.57	0.55	0.55
2098	0.88	0.84	0.81	0.78	0.77	0.78	0.79
2100	0.83	0.80	0.78	0.73	0.70	0.70	0.70
2134	0.83	0.78	0.73	0.68	0.66	0.66	0.66
2136	0.84	0.78	0.73	0.68	0.65	0.64	0.64
2164	0.74	0.65	0.56	0.49	0.46	0.46	0.47

Columns: (1) Cluster designation. (2) to (8) Continuum intensity relative to that at 5870 Å.

4. Ranking cluster ages

In order to study the integrated light evolution in the near-infrared we need an age ranking of the clusters which should be as free as possible from the contamination of cool stars. Ages from the turn-off point are available for $\approx 50\%$ of the clusters in our sample, according to Hodge's compilation (1983), complemented with Hodge (1982) for the oldest cluster in the sample, the blue/red transition cluster NGC 1868 for which we adopt an age of 500 Myr. Hodge's calibration is based on classical models of stellar evolution. The use of a scale based on models incorporating convective overshooting leads to ages a factor three larger on average for blue clusters (Chiosi et al., 1989). For the present purposes, however, the fundamental point is the age ranking so we simply adopt the classical calibration.

For the clusters without measured HR diagram it is necessary to use age indicators from the integrated light. Ideally one should use the ultraviolet range from IUE spectra, where the contamination from cool stars is negligible for young clusters (Cohen et al., 1984; Barbero et al., 1989). Unfortunately Hodge's clusters in our sample are essentially the same as those observed with IUE, so we are left with the blue-violet colours in order to estimate ages for the rest of the sample. In Table 1 we give Johnson's $(U-B)_0$ colour, corrected for the foreground reddening values given in Sect. 2, from the data in Van den Bergh (1981). Figure 5a shows $(U-B)_0$ vs. log (age Myr^{-1}), for which a linear regression gives

$$(U-B)_0 = 0.52 \log (\text{age Myr}^{-1}) - 1.09 \qquad (1)$$

with $\sigma = 0.08$ mag.

The $(B-V)_0$ colour is not suitable because in the V filter the flux contribution from red stars is still important. This explains why NGC 2002, a cluster with a strong red supergiant content (Sect. 5) is as red in this colour as the blue/red transition cluster NGC 1868 (Table 1).

The photometry of SWB 80 gave origin to the SWB classification, of which our clusters basically span types I to IV (Table 1);

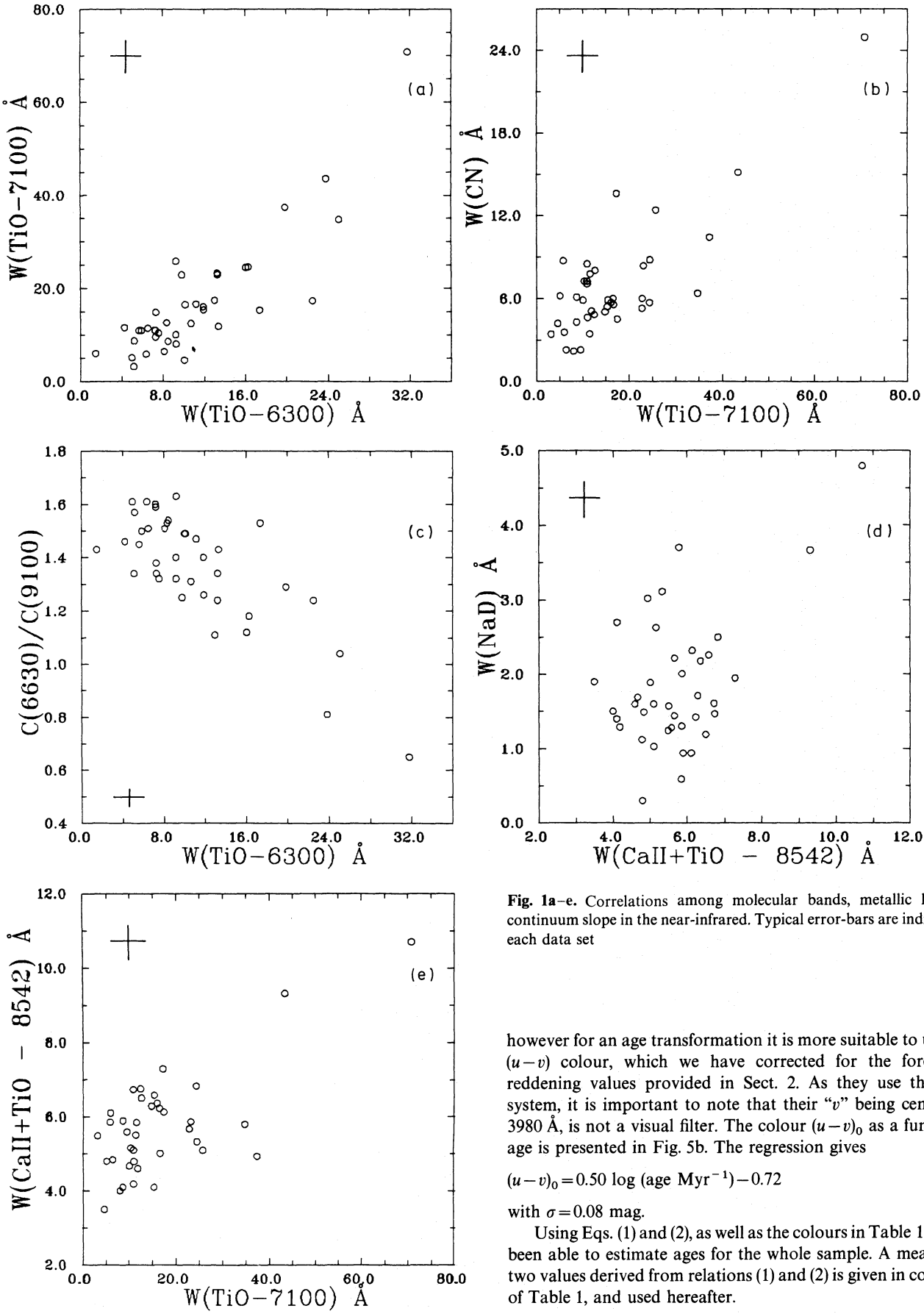

Fig. 1a–e. Correlations among molecular bands, metallic lines and continuum slope in the near-infrared. Typical error-bars are indicated for each data set

however for an age transformation it is more suitable to use their $(u-v)$ colour, which we have corrected for the foreground reddening values provided in Sect. 2. As they use the Gunn system, it is important to note that their "v" being centered at 3980 Å, is not a visual filter. The colour $(u-v)_0$ as a function of age is presented in Fig. 5b. The regression gives

$$(u-v)_0 = 0.50 \log (\text{age Myr}^{-1}) - 0.72 \qquad (2)$$

with $\sigma = 0.08$ mag.

Using Eqs. (1) and (2), as well as the colours in Table 1 we have been able to estimate ages for the whole sample. A mean of the two values derived from relations (1) and (2) is given in column 10 of Table 1, and used hereafter.

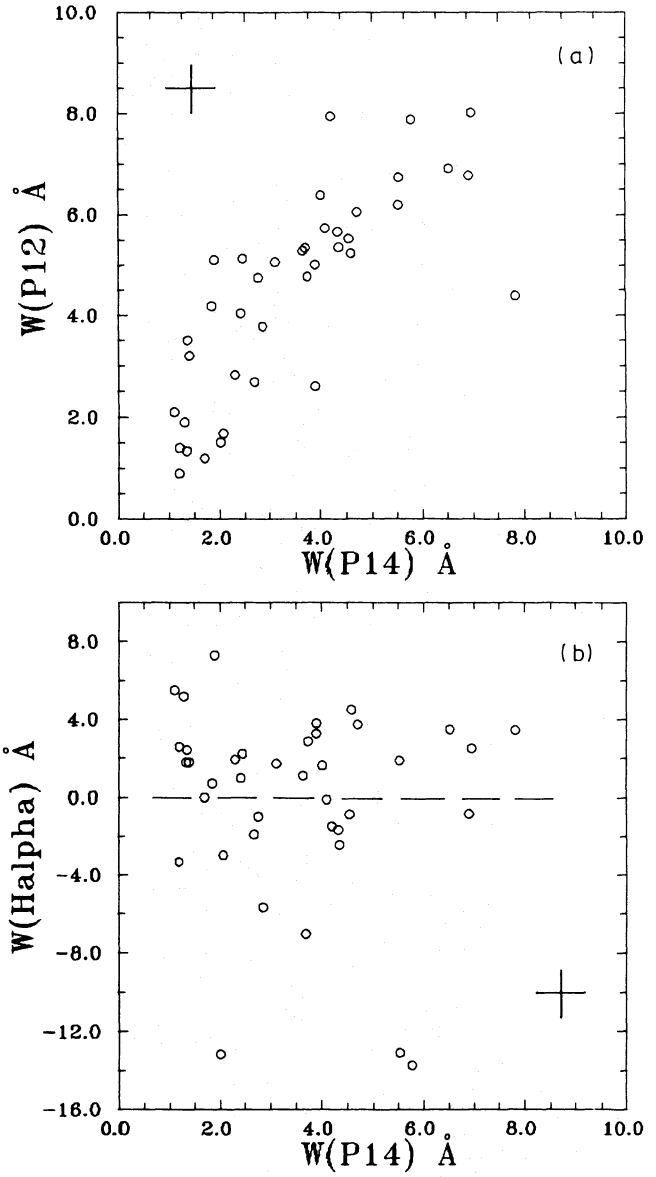

Fig. 2a and b. Comparison of hydrogen lines: **a** Paschen 12 vs. Paschen 14; **b** Hα vs Paschen 14, negative values correspond to emission

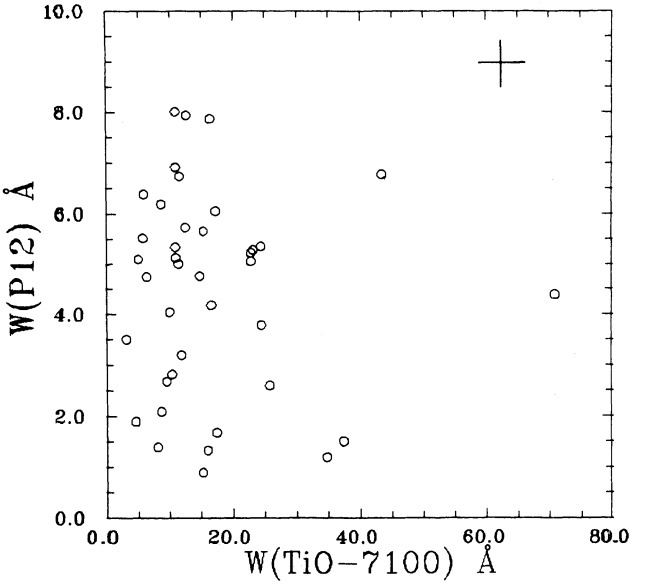

Fig. 3. Comparison of unblended features arising from hot and cool stars: they show no correlation

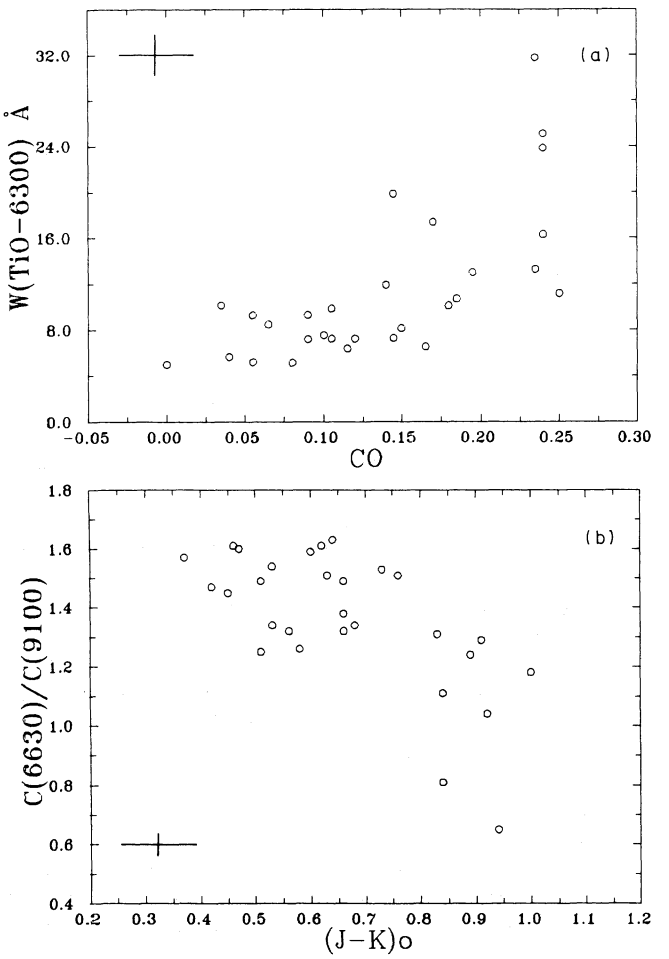

Fig. 4a and b. Comparison of near-infrared indices with colours and line indices from the infrared photometry by Persson et al. (1983)

5. Near-infrared spectral evolution

We analyze the main features as a function of age by defining some representative indices. The average $\langle W(\mathrm{TiO})\rangle$ of the bands at $\lambda \approx 6000$, 6300 and 7100 Å is shown in Fig. 6a as a function of age. The large values of W(TiO) for the age range 7–12 Myr confirms the existence of the red supergiant phase. The occurrence of this phase is also clear from the near-infrared spectral slope as defined by the continuum ratio C(6630 Å)/C(9100 Å) depicted in Fig. 6b. From these results we have been able to identify new clusters experiencing the red supergiant phase, whose spectra are shown in Fig. 7, in addition to the previously known case of NGC 2004. The red supergiant contribution is so strong in NGC 1805 and NGC 2002, that the cluster continuum slope is positive for $\lambda > 6000$ Å (in λ units).

Figures 6a and 6b also indicate that the two new clusters with ages similar to that of NGC 1866 (≈ 100 Myr) present also an

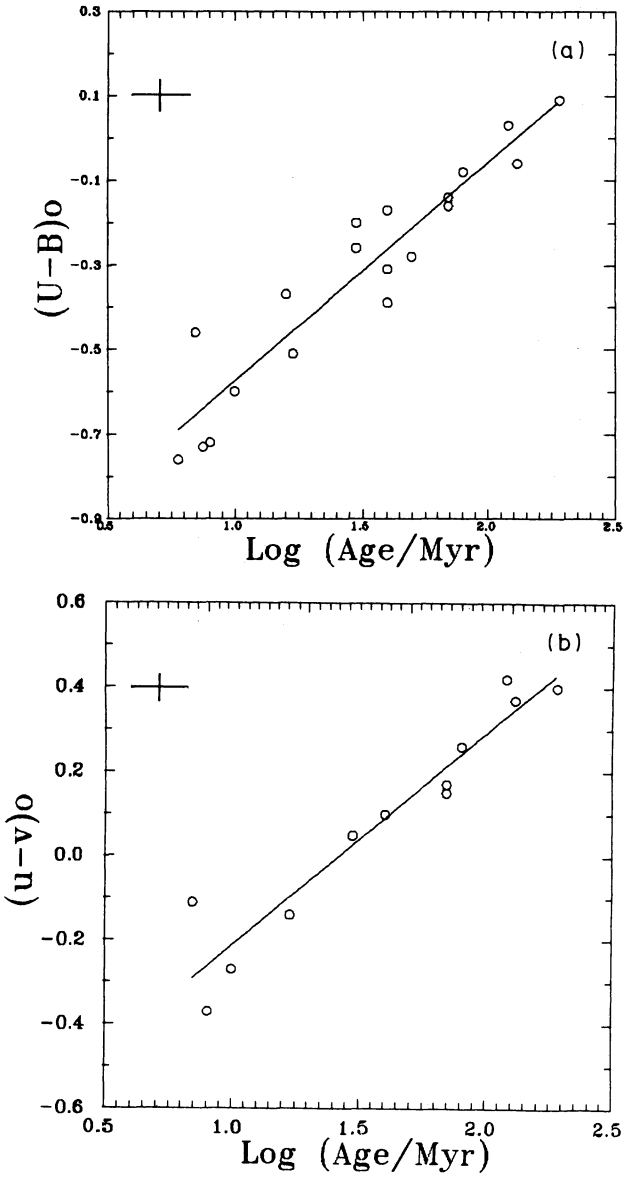

Fig. 5a and b. Correlations between blue-violet colours and turn-off ages. **a** $(U-B)_0$ colour; **b** Gunn $(u-v)_0$ colour

important red stellar content, presumably associated with AGB stars.

The age dependence of $W(\mathrm{H}\alpha)$ is shown in Fig. 8. Hα appears as a strong emission line from $t \approx 10$ to 50 Myr. As pointed out in Sect. 1, Hα originates mostly from stellar sources. Most of these are Be stars which are present in Galactic disc clusters of similar ages (Mermilliod, 1981a,b). We emphasize at this point that the present groups of integrated cluster spectra for the LMC are strongly related to the composite HR diagrams of Galactic open clusters at similar age intervals given by Mermilliod, both in terms of emission and red stellar content.

Considering the evolution with age of the absorption and of the emission features in the blue LMC clusters we have grouped them into 8 classes in order to generate templates for population synthesis. The properties of these groups are given in Table 4 and the corresponding spectra are shown in Fig. 9a. We have doubled the number of groups with respect to those in Bica (1988) for the

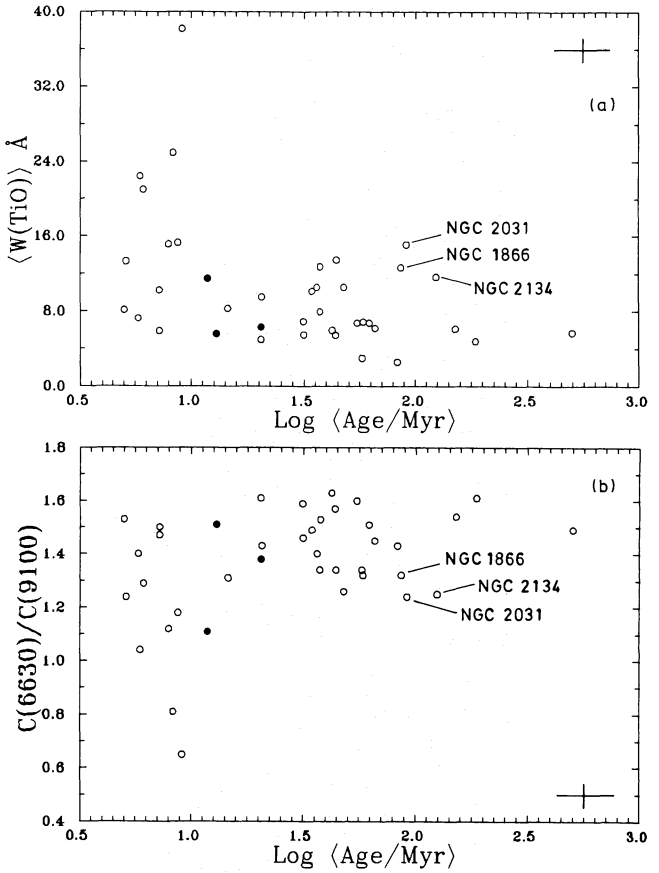

Fig. 6a and b. Age dependence of: **a** TiO strength; **b** Continuum slope. Open circles represent LMC clusters and black dots represent SMC clusters

same age range (Y1, Y2, Y3, Y4). We replace them by new designations Y_A to Y_H in the new sequence:

(i) Y_A is a new class between the pure H II region phase and the red supergiant phase ($Y1 = Y_B$). In Y_A a cluster has not yet significantly developed its red supergiant phase while it is essentially free of line emission. Y_B corresponds to the full development of the red supergiant phase.

(ii) We break up the former group Y2 into new groups Y_C, Y_D and Y_E. A more important cool stellar content appears in Y_D relative to its neighbours, Y_C and Y_E, but this might result from statistical fluctuations because $\langle W(\mathrm{TiO})\rangle$ and the continuum slope (Fig. 7) present a large scatter in the corresponding age range ($1.54 < \log \text{age Myr}^{-1} < 1.70$). The groups Y_B and Y_C have strong Hα in emission which, as just discussed, originates from stars rather than from extended gas; for group Y_D, Hα in emission and absorption almost cancel out, suggesting the end of the Be star phase in the cluster evolution. For older ages line emission, extended or stellar, has completely disappeared.

(iii) As already pointed out in BA86 and BA87 concerning NGC 1866, there appears to be another red phase around 100 Myr, presumably related to AGB stars. The two new entries with similar age, NGC 2031 and NGC 2134, exhibit the same effect. Consequently we confirm the need for breaking up our previous group Y3 into two classes Y_F (with red flux excess) and Y_G (bluer again like Y_E). Finally we have the case of NGC 1868, which corresponds to the blue/red integrated colour transition possibly associated to the development of the giant branch (Renzini and

Table 4. Groups and equivalent widths from low continuum tracings

(1) Group	(2) Members NGC	(3) Age (Myr)	(4) P 17 8467	(5) Ca II-8498 + P 16-8502	(6) Ca II-8542 + P 15-8545	(7) P 14 8598	(8) Ca II-8662 + P 13-8665	(9) P 12 8751
Y_A. LMC	1767 2003 2006 SL 538 2011	5–7	1.1	1.9	4.1	1.7	2.9	1.5
Y_B. LMC	1805 1994 2002 2004 2098 2100	7–12	0.9	2.2	5.0	1.2	4.0	1.2
Y_C. LMC	1711 1735 1818 1847 1850 1854	12–35	0.9	1.8	3.6	1.3	3.5	2.2
Y_D. LMC	1774 1782 1903 1951 2157 2164 2214	35–50	1.0	1.7	4.4	1.8	4.5	1.3
Y_E. LMC	1755 2025 2041 2058 2065 2136	50–85	1.0	2.1	4.5	1.5	3.1	1.8
Y_F. LMC	1866 2031 2134	85–130	1.0	2.6	4.2	2.2	3.8	1.2
Y_G. LMC	1831 1856	130–250	1.4	1.9	4.3	2.0	4.8	2.0
Y_H. LMC	1868	250–750	0.7	1.8	3.3	1.4	3.7	1.2
Y_B. SMC	299	12	0.9	2.1	5.6	1.1	3.2	1.2
Y_C. SMC	330 376	13–20	1.1	1.8	4.6	1.8	3.1	2.3

Columns: (1) LMC and SMC spectral groups: (2) Star clusters in the group; (3) Age range; (4) to (9) Equivalent Widths in Angstroms for Paschen and Ca II lines from low continuum tracings in order to avoid molecular absorption contamination. Estimated errors are on average 8%.

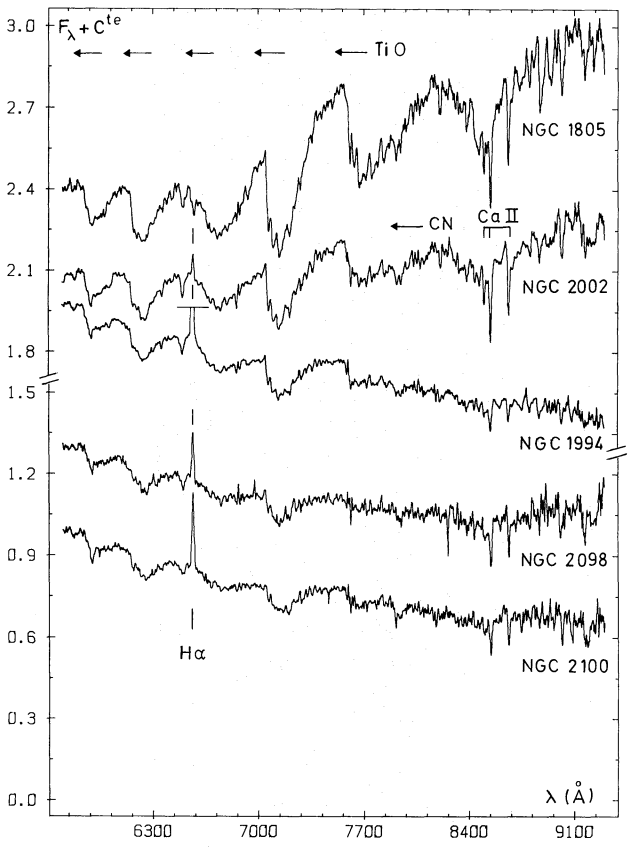

Fig. 7. LMC clusters in the red supergiant phase

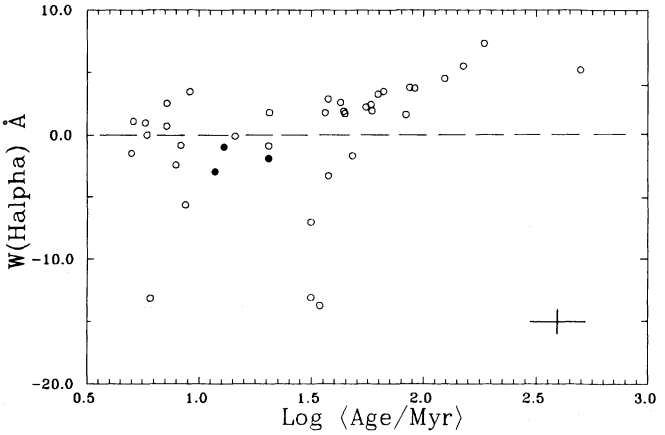

Fig. 8. Age dependence of Hα. Open circles represent LMC clusters and black dots SMC clusters

Buzzoni, 1986). It does not differ significantly from group Y_G in the near-infrared, but it is clearly redder in the blue spectral range and must be kept as a separate group ($Y4 = Y_H$). A possibly new cluster in this group is NGC 2249, according to its *UBV* colours (Van den Bergh, 1981).

Table 4 also contains the 3 SMC clusters classified into two groups, the metal-poor counterparts of Y_B and Y_C in the LMC. The SMC spectral groups are shown in Fig. 9b. NGC 299 pertains to the red supergiant phase, because it has a flat spectrum and strong Ca II triplet. However, the molecular bands are weak owing to the low metallicity of the SMC. The strength of molecular bands in general shows non-linear dependences with

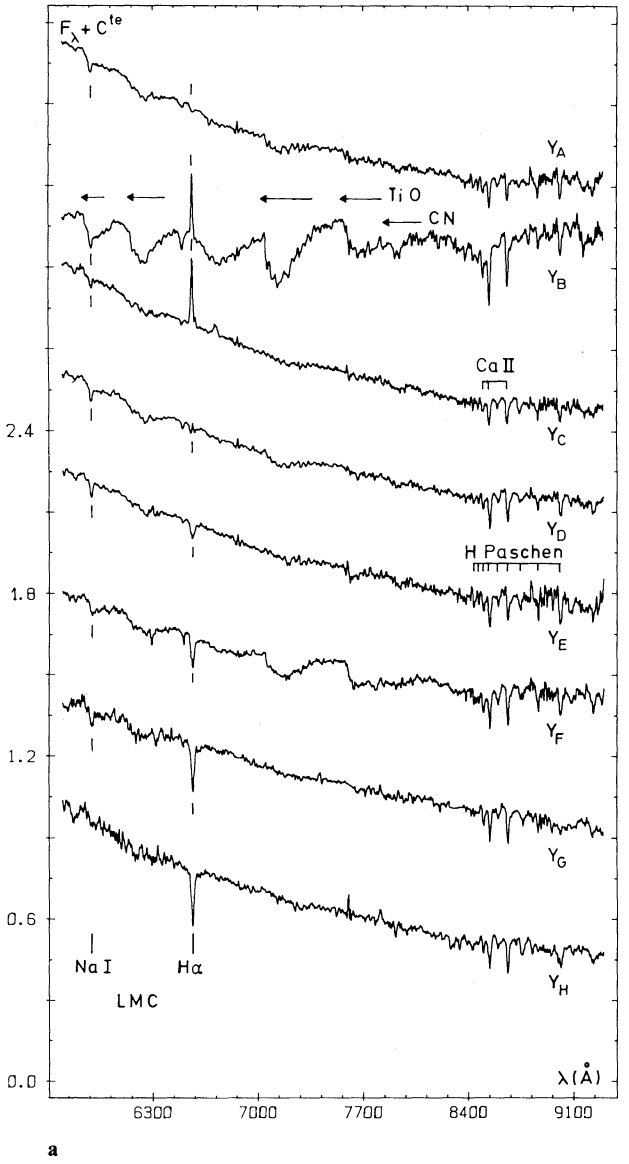

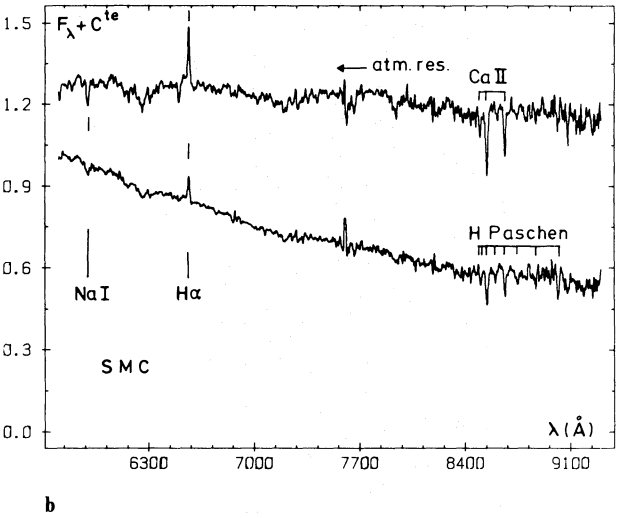

Fig. 9a and b. Spectral evolution: **a** LMC groups; **b** SMC groups

metallicity, increasing quite fast for $[Z/Z_\odot] > -0.5$. Conversely, atomic lines like Ca II present linear dependences on $[Z/Z_\odot]$, and even in metal poor clusters they are relatively stronger than the molecular bands. We conclude that the behaviours of molecular bands in the young LMC and SMC clusters are clearly those of stellar populations with metallicities slightly above and below $[Z/Z_\odot] = -0.5$, respectively. The SMC clusters NGC 330 and NGC 376 appear to be in a blue phase like those in the LMC group Y_C.

We also provide in Table 4 measurements of the Ca II triplet lines and the neighbouring Paschen lines, considering local, lower continuum tracings in order to minimize the contribution from TiO molecular bands. This procedure is suitable for studying the possible enhancement of the Ca II triplet when low gravity stars are present, such as red supergiants (Jones et al., 1984; Alloin and Bica, 1989; Diaz et al., 1989; Smith and Drake, 1990). We show in Figs. 10a and 10b the time-evolution of the total W(Ca II) respectively non-corrected and corrected for the superimposed Paschen lines. The presence of the red supergiants is obvious, particularly in the Paschen-free plot. Interpretation of the figures for clusters outside the red supergiant phase would require a detailed population synthesis which is beyond the scope of this study. We simply point out that these results address interesting questions such as the formation of the low part of the main sequence in young clusters and the first appearance of AGB stars.

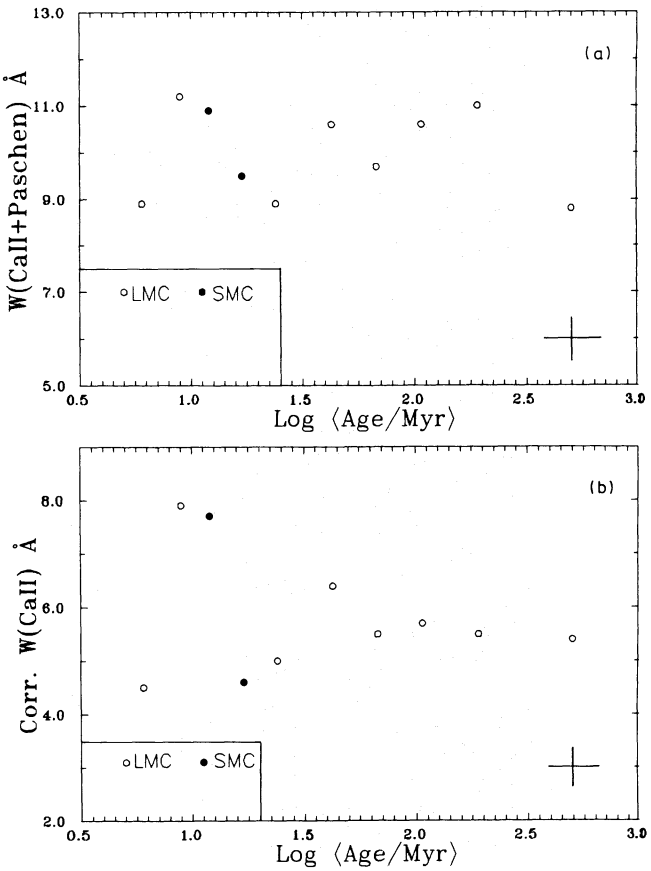

Fig. 10a and b. Evolution of the Ca II triplet free of TiO contamination: **a** blended with Paschen lines. **b** corrected for Paschen lines. Open circles represent LMC clusters and black dots represent SMC clusters

6. Concluding remarks

The near-infrared spectral analysis of 39 among the brightest and largest blue Magellanic clusters provides the following conclusions:

(i) The red supergiant phase is now well-documented in the LMC cluster evolution at $t \approx 10$ Myr. NGC 299 in the SMC is also a clear example of it, although molecular bands are then weaker owing to the SMC metal deficiency.

(ii) Three clusters at $t \approx 100$ Myr show as well a strong red stellar component, which might be associated to an enhancement in the flux from AGB stars.

(iii) Only the most massive clusters appear to have been able to keep some gas from their formation period.

(iv) The Hα emission is strongest between 10 and 50 Myr and appears to arise mostly from stellar sources. These are likely Be stars, a phenomenon which is also common in Galactic open clusters of similar age.

(v) We have identified 8 stages in the cluster near-infrared spectral evolution between 5 and 500 Myr, which in conjunction with other wavelength ranges, will be very useful for modeling the stellar populations in star-forming galaxies.

(vi) A detailed analysis of the Ca II triplet after elimination of molecular and Paschen contaminations clearly shows its prominence during the red supergiant phase. This results from the low surface gravity of the light-dominant stars.

Finally, we point out that it would be of great importance to derive for the SMC and the disc of M 31, spectral evolution sequences complementary to the one we have constructed for the LMC clusters. This would create a solid base for young population synthesis in three metallicity ranges.

Acknowledgements. We are indebted to the ESO staff at La Silla and Garching for assistance. We thank J. Cohen and J. Lequeux for useful comments. E.B. and J.S. acknowledge grants from the Brazilian Institution CNPq.

References

Alloin, D., Bica, E.: 1989, *Astron. Astrophys.* **217**, 57
Arimoto, N., Bica, E.: 1989, *Astron. Astrophys.* **222**, 89
Barbero, J., Brocato, E., Cassatella, A., Castellani, V., Geyer, E.: 1989, *ESO preprint* no. **643**
Bica, E.: 1988, *Astron. Astrophys.* **195**, 76
Bica, E., Alloin, D.: 1986, *Astron. Astrophys.* **162**, 21
Bica, E., Alloin, D.: 1987, *Astron. Astrophys.* **186**, 49
Bica, E., Alloin, D.: 1988, in *Towards Understanding Galaxies at Large Redshifts*, eds. R.G. Kron, A. Renzini, Kluwer, Dordrecht, p. 77
Chiosi, C., Bertelli, G., Bressan, A.: 1988, *Astron. Astrophys.* **196**, 84
Cohen, J.G.: 1982, *Astrophys. J.* **258**, 143
Cohen, J.G., Rich, R.M., Persson, S.E.: 1984, *Astrophys. J.* **285**, 595
Davies, R., Elliot, K., Meaburn, J.: 1979, *Mem. Roy. Astron. Soc.* **81**, 89
Diaz, A., Terlevich, E., Terlevich, R.: 1989, *Monthly Notices Roy. Astron. Soc.* **239**, 325
Freeman, K., Illingworth, G., Oemler, A.: 1983, *Astrophys. J.* **277**, 488
Henize, K.: 1956, *Astrophys. J. Suppl.* **2**, 315
Hodge, P.: 1961, *Astrophys. J.* **133**, 413
Hodge, P.: 1982, *Astrophys. J.* **256**, 477
Hodge, P.: 1983, *Astrophys. J.* **264**, 470
Jones, J., Alloin, D., Jones, B.: 1984, *Astrophys. J.* **283**, 457
Mermilliod, J., 1981a: *Astron. Astrophys.* **97**, 235
Mermilliod, J., 1981b: *Astron. Astrophys. Suppl.* **44**, 467
Mould, J., Aaronson, M.: 1980, *Astrophys. J.* **240**, 464
Persson, S., Aaronson, M., Cohen, J., Frogel, J., Matthews, K.: 1983, *Astrophys. J.* **266**, 105
Renzini, A., Buzzoni, A.: 1986, in *Spectral Evolution of Galaxies*, eds. C. Chiosi, A. Renzini, Reidel, Dordrecht, p. 135
Searle, L., Wilkinson, A., Bagnuolo, W.: 1980, *Astrophys. J.* **239**, 803
Smith, G., Drake, J.: 1990, *Astron. Astrophys.* (in press)
Van den Bergh, S.: 1981, *Astron. Astrophys.* **46**, 79